U.S. DEPARTMENT OF THE INTERIOR
U.S. GEOLOGICAL SURVEY

URANIUM-SERIES ANALYSES OF EVAPORITES FROM THE 1000-FOOT PAN-3 CORE, PANAMINT VALLEY, CALIFORNIA

by

John A. Fitzpatrick, James L. Bischoff and George I. Smith

Menlo Park, CA

Open-File Report 93-558

1993

INTRODUCTION

Periodically during the last 3.0 m.y., the Owens River drainage system has consisted of a chain of large lakes occupying a succession of closed basins in southeastern California (Fig. 1). Presently, the location of these paleo-lakes is marked by playas or small saline lakes, but evidence of previous higher lake levels is provided by lacustrine deposits and wave-cut terraces found at various elevations within the basins. The lakes were supplied predominantly by the Owens River which presently drains an area of about 8500 km^2, but receives most of its runoff from the eastern slope of the Sierra Nevada. At any given time the number of lakes in the chain and the size of the terminal lake are constrained by the regional climate. During historic times, Owens Lake has been the terminus of the system, but during wetter periods of the past Owens Lake has overflowed to progresssively fill a series of lower basins: China Lake, Searles Lake, Panamint Lake, and Death Valley Lake. Throughout much of the past million years, Searles Lake was the terminus of the system, but during extreme pluvial episodes Searles Lake overflowed to supply Panamint Lake and rarely Panamint overflowed into Death Valley Lake (G.I. Smith, 1984).

At its overflow level, Panamint Lake had an area of about 300 square miles, a depth of over 950 feet, and a volume of about 92 million acre feet. The elevation of the high stand was controlled by overflow into Death Valley through Wingate Pass (elevation=1977±1 feet). R. S. Smith (1976) has identified at least five uplifted lake terraces and associated lacustrine deposits which correspond with high-stand overflow events. Fitzpatrick and Bischoff (1993) have performed U-series analysis on lacustrine deposits from a number of Panamint high shorelines. Evidence for low and intermediate stands of the lake is also seen in a number of locations in the valley (Smith, 1976).

Smith and Pratt (1957) have characterized the sedimentary deposits in Panamint Valley from cores drilled in 1953. The PAN-3 core (Fig. 2) was removed from a 1000 foot-thick sequence of clastic sediments with two thick interbedded units of pure halite. The halite deposits represent periods of lake desiccation, indicating a period during which evaporation exceeded precipitation and inflow. The timing of these desiccation events is important for the reconstruction of the lacustrine and climatic history of the Owens drainage basin. Bischoff et al. (1985) successfully dated a series of salt samples from the LDW-6 core in Searles Lake, adding important age control to the sedimentary record from that lake, the immediate upstream water source for Panamint Lake. Jannik et al. (1991) report three ^{36}Cl dates from the PAN-3 core in a study of Pleistocene sedimentation in the Owens River system. The present study was undertaken to establish further age control for the PAN-3 sedimentary sequence by application of uranium-series dating. Our new dates allow a broad definition of sedimentation rates within Panamint Lake over the past 350

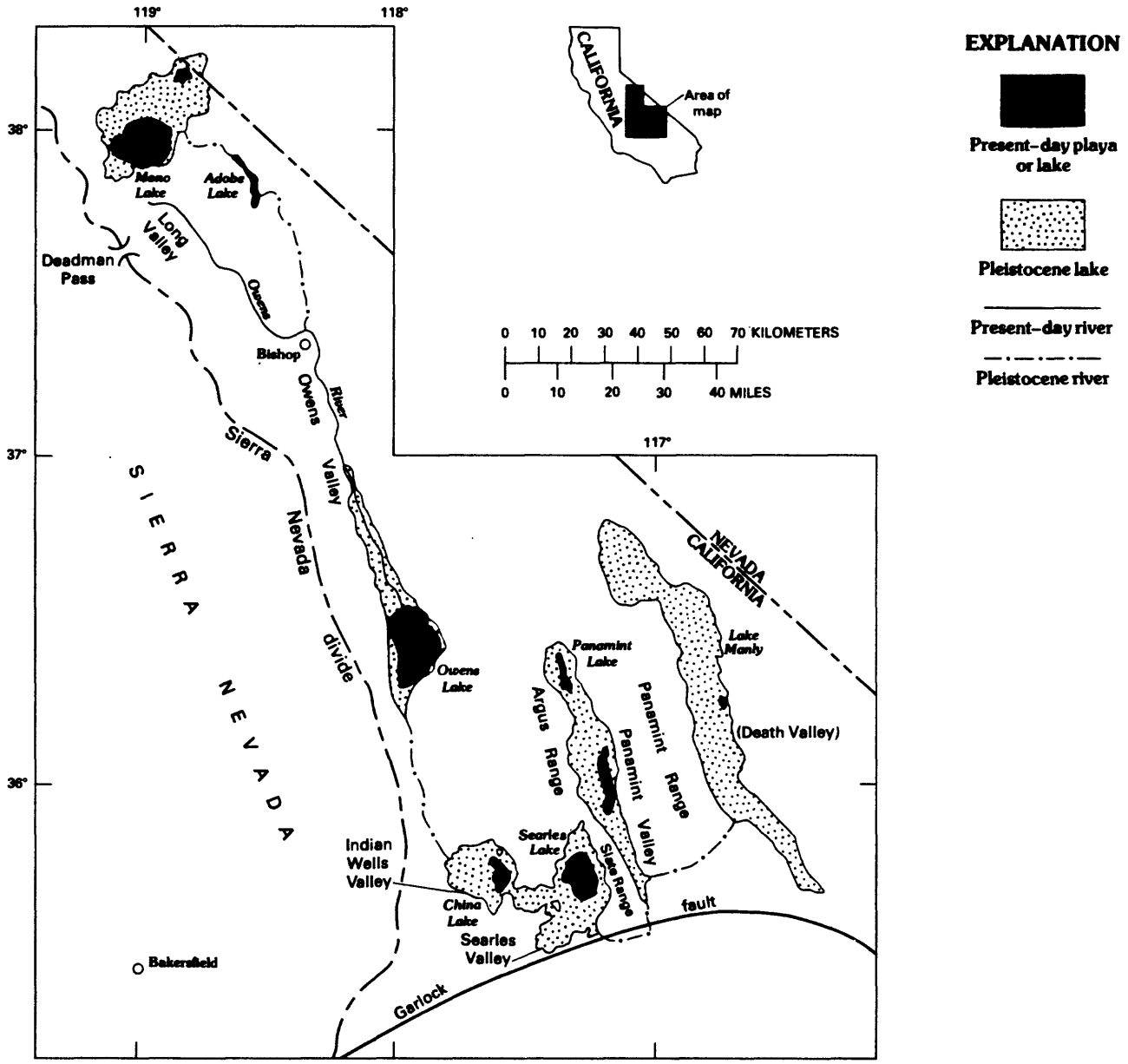

Figure 1

Owens River System and chain of Pleistocene Lakes

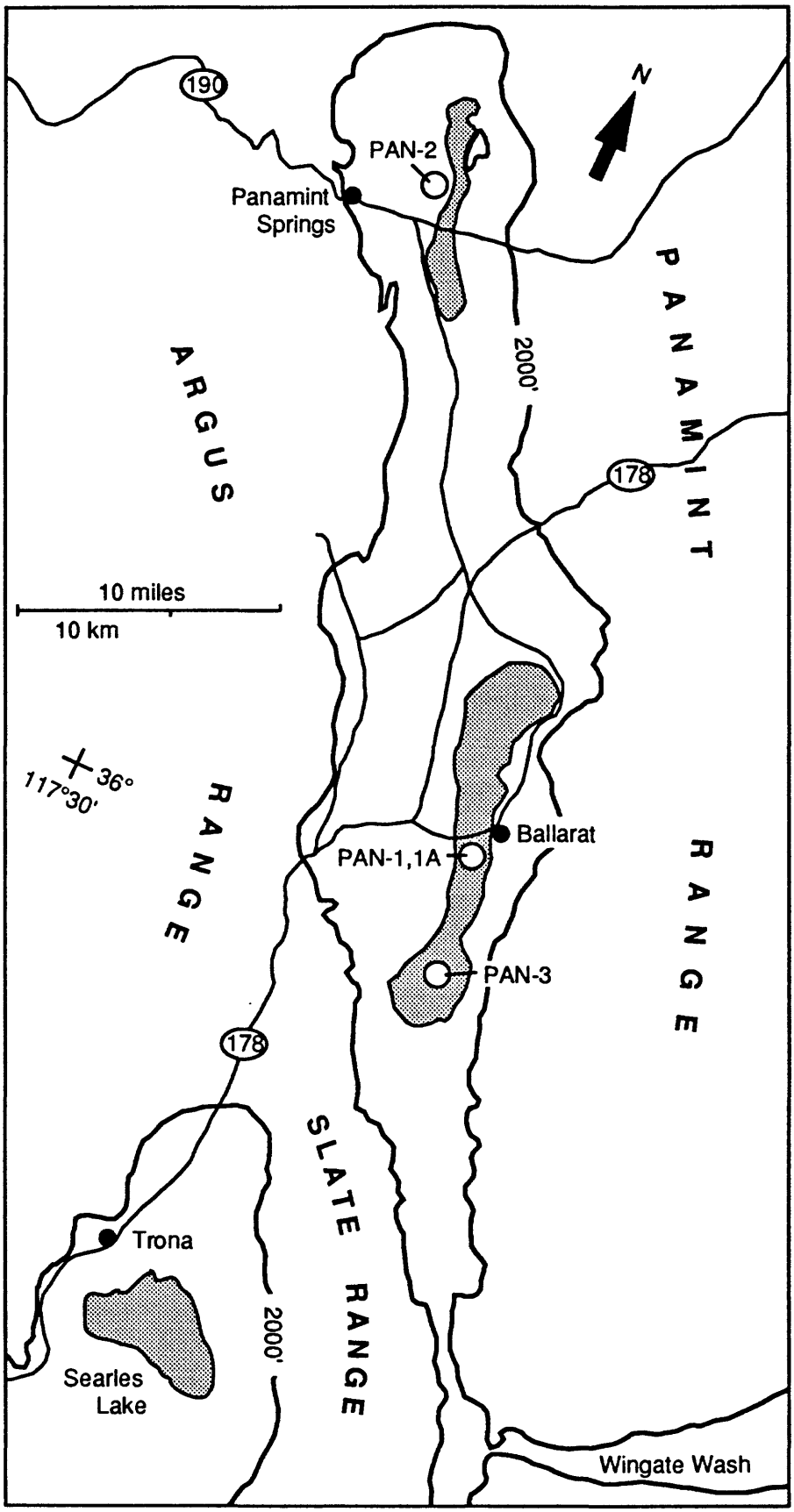

Figure 2
Sketch map of Panamint Valley showing locations of holes drilled and cores obtained by Smith and Pratt (1957).

Table 1
Uranium and thorium isotopic analyses and derived dates of various sediments from the PAN-3 core, Panamint Valley, California

Depth (ft.)	lab no.	U ppm	$^{234}U/^{238}U$	$^{230}Th/^{232}Th$	date (ka)	notes
49.8	91-56	3.00±0.05	1.22±0.01	8.25±0.56	20±1	leachate
80.7	91-58	0.16±0.01	1.35±0.06	2.63±0.26	47±4	leachate
80.7	91-107	0.19±0.01	1.32±0.03	1.82±0.07	48±2	TD, x>30
80.7	91-108	0.21±0.01	1.21±0.04	1.93±0.08	47±2	TD, 100<x<30
80.7	91-109	0.42±0.01	1.19±0.03	1.98±0.07	54±2	TD, x<100
						Isochron=39±8
82.0	91-117	0.46±0.02	1.25±0.05	2.77±0.23	37±3	leachate
90.0	91-102	5.92±0.16	1.23±0.01	34.68±2.18	21±1	TD, x<200
90.0	91-103	3.28±0.09	1.22±0.02	22.60±1.41	24±1	TD, 200<x<100
90.0	91-104	1.80±0.04	1.24±0.02	50.45±4.59	20±1	TD, 100<x<30
90.0	91-105	1.51±0.03	1.22±0.02	38.33±3.68	22±1	TD, x>30
90.0	91-106	1.77±0.03	1.23±0.01	11.79±0.55	25±1	TD, bulk
90.0	91-110	2.02±0.04	1.22±0.02	30.21±3.91	23±1	leachate
90.0	91-118	3.82±0.12	1.20±0.02	20.29±1.66	22±1	leachate
						Isochron=19±1
131.0	91-119	0.62±0.02	1.19±0.04	7.77±0.61	73±5	leachate
131.0	91-141	1.30±0.04	1.21±0.03	6.36±0.31	69±4	TD, bulk
131.0	91-142	0.22±0.01	1.16±0.04	11.52±1.17	63±4	leachate
						Isochron=55±7
135.0	91-120	0.14±0.01	1.27±0.08	>1000	60±6	leachate
135.0	91-135	0.14±0.01	1.19±0.02	9.17±0.41	72±3	leachate
162.0	91-59	0.11±0.01	1.00±0.06	0.92±0.05	>350	leachate
165.0	91-121	0.18±0.01	1.15±0.09	3.60±0.44	58±7	leachate
180.0	91-122	0.04±0.00	1.65±0.22	1.74±0.24	131±32	leachate

Depth (ft.)	lab no.	U ppm	$^{234}U/^{238}U$	$^{230}Th/^{232}Th$	date (ka)	notes
190.0	91-123	0.80±0.03	1.13±0.04	12.53±1.32	123±13	leachate
190.0	91-143	0.80±0.02	1.15±0.02	9.72±0.33	98±4	TD, sample A
190.0	91-144	0.86±0.02	1.15±0.02	14.02±0.58	95±3	TD, sample A
190.0	91-145	0.25±0.01	1.14±0.03	4.05±0.17	121±7	TD, sample B
190.0	91-146	0.57±0.01	1.16±0.02	9.51±0.40	93±3	TD, sample C
						Isochron=92±18
205.0	91-60	0.48±0.01	1.09±0.03	2.54±0.11	128±10	leachate
205.0	91-61	0.49±0.01	1.16±0.02	2.38±0.05	121±5	TD, x>70
205.0	91-62	0.41±0.01	1.16±0.02	2.50±0.07	119±6	TD, 70<x<30
205.0	91-63	1.96±0.03	1.12±0.02	2.21±0.03	141±6	TD, x<200
205.0	91-64	0.55±0.01	1.17±0.03	2.44±0.07	125±7	TD, 100<x<70
205.0	91-65	0.88±0.02	1.14±0.03	2.16±0.06	138±9	TD, 200<x<100
						Isochron=69±11
214.0	91-132	0.14±0.01	1.01±0.03	0.95±0.03	202±24	leachate
224.5	91-136	0.10±0.01	0.90±0.07	0.84±0.06	153±34	leachate
239.5	91-156	0.20±0.01	1.08±0.02	8.59±0.43	149±9	TD, sample A
239.5	91-157	0.58±0.01	1.15±0.02	7.16±0.19	152±7	TD, sample B
239.5	91-158	0.22±0.01	1.20±0.03	4.57±0.22	115±6	TD, sample C
						Isochron=260±105
249.0	91-133	0.19±0.01	1.14±0.03	2.67±0.09	109±5	leachate
265.0	91-75	0.16±0.01	1.14±0.05	1.46±0.06	177±22	leachate
265.0	91-111	0.19±0.01	1.10±0.02	1.58±0.04	206±15	TD, bulk
265.0	91-112	0.13±0.01	1.12±0.03	1.78±0.06	166±11	TD, x>30
265.0	91-113	0.15±0.01	1.12±0.03	1.50±0.04	163±11	TD, 100<x<30
265.0	91-115	0.36±0.01	1.10±0.04	1.51±0.04	217±26	TD, x<200
265.0	91-116	0.20±0.01	1.16±0.06	1.53±0.07	184±24	TD, 200<x<100
						Isochron=83±38

Depth (ft.)	lab no.	U ppm	$^{234}U/^{238}U$	$^{230}Th/^{232}Th$	date (ka)	notes
376.2	91-81	2.72±0.05	1.05±0.02	0.87±0.01	>350	leachate
395.0	91-82	2.88±0.04	1.08±0.01	2.17±0.03	214±13	TD, bulk
395.0	91-83	2.62±0.05	1.05±0.02	1.87±0.03	200±14	leachate
395.0	91-92	2.11±0.04	1.11±0.02	1.95±0.03	298±42	TD, 200<x<100
395.0	91-93	3.85±0.08	1.08±0.02	1.84±0.03	342±74	TD, x<200
395.0	91-94	1.63±0.04	1.15±0.03	1.81±0.04	265±31	TD, 100<x<30
395.0	91-95	3.08±0.06	1.12±0.02	1.89±0.03	339±69	TD, x>12
395.0	91-96	2.95±0.06	1.09±0.02	1.83±0.03	306±53	TD, 30<x<12
						Isochron=91±17
445.0	91-134	1.24±0.02	1.09±0.01	16.95±0.64	347±78	leachate
445.0	91-147	1.15±0.02	1.06±0.02	15.74±0.80	284±36	TD, sample A
445.0	91-148	0.54±0.01	1.17±0.03	15.64±1.09	223±21	TD, sample B
445.0	91-149	1.12±0.02	1.11±0.02	13.96±0.63	265±30	TD, sample C
						Isochron=161±150
470.0	91-124	3.10±0.12	1.10±0.03	10.26±0.48	295±119	leachate, sample A
470.0	91-150	2.48±0.35	1.11±0.02	10.91±0.30	310±33	TD, sample A
470.0	91-151	1.34±0.02	1.11±0.02	14.59±0.65	326±51	TD, sample B
470.0	91-152	1.25±0.02	1.12±0.02	16.25±0.82	331±52	TD, sample B
						Isochron=>350
470.3	91-153	0.31±0.01	1.13±0.02	13.23±0.45	>350	TD, sample A
470.3	91-154	0.34±0.01	1.15±0.02	20.40±1.30	305±49	TD, sample B
470.3	91-155	0.19±0.01	1.07±0.02	15.53±0.92	313±59	TD, sample C
						Isochron=234±100
510.0	91-127	3.05±0.11	1.15±0.02	93.87±12.51	216±37	leachate
510.0	92-4	3.26±0.10	1.08±0.03	89.07±11.50	325±112	leachate
525.0	92-5	6.73±0.14	1.12±0.02	49.82±3.11	>350	leachate
526.0	91-76	4.08±0.10	1.09±0.01	37.27±1.49	>350	leachate

k.y. but do not offer the precision required to make fine-scale sedimentologic and climatic interpretations.

SAMPLES AND PROCEDURES

Uranium-series analyses were performed on a number of evaporite samples from the PAN-3 core, located in the south playa of Panamint valley (Fig. 2). The sample suite consists entirely of halite with the exception of two gypsum samples taken at 376.2 ft. and 395.0 ft. The PAN-3 core was drilled in 1953 (Smith and Pratt, 1957) and stored dry thereafter. Although preservation has not been ideal, sample lithologies and locations match quite well with the lithologies originally logged. Samples were mechanically cleaned of visible detritus, then crushed and subdivided by grain size into several sample splits (>30 mesh, 30-100 mesh, 100-200 mesh, and <200 mesh). Leachate analyses were performed on the bulk sample by dissolution in 2 N HNO_3. Total sample dissolutions (TD) were performed on a number of samples in order to construct isochrons (Bischoff and Fitzpatrick, 1991). Discrete bulk samples or grain-size subdivisions were completely dissolved in a mixture of HNO_3 and HF in order to dissolve both authigenic and detrital silicate phases. For both the leachate and TD analyses, uranium and thorium isotopes were separated by ion-exchange chromatography and solvent extraction (Bischoff et al., 1988) and analyzed by alpha spectrometry.

RESULTS AND DISCUSSION

The results of the uranium-series analyses are shown in Table 1. Uranium contents among samples are extremely variable, ranging between 0.04 to 6.7 ppm. Similarly, $^{230}Th/^{232}Th$ ratios exhibit a wide range of values (0.8 to >1000), and the $^{234}U/^{238}U$ ratios range between 0.90 to 1.65 for all samples. Samples 91-59, 91-122, 91-132, and 91-136 are problematic, in that they all have very low U contents, low $^{230}Th/^{232}Th$ ratios, and unusual $^{234}U/^{238}U$ ratios. Although these samples had negligible amounts of insoluble residue, the isotopic analyses suggest that these salts contained almost no authigenic uranium and the results represent isotopic transfer from the associated detrital fraction. Replicate analyses of individual samples and of the separate size fractions exhibit broadly similar values for U content, $^{230}Th/^{232}Th$ ratios, and $^{234}U/^{238}U$ ratios. The 90-ft sample, for instance, shows U contents ranging between 1.5 to 5.9 ppm, $^{230}Th/^{232}Th$ ratios ranging between 11.8 to 50.5, and $^{234}U/^{238}U$ ratios ranging between 1.20 to 1.24.

Figure 3

Nominal date versus depth plot for all samples from the PAN-3 core. Sedimentation-rate curves of 1.2 ft/kyr and 2 ft/kyr are shown as likely maximum and minimum limits.

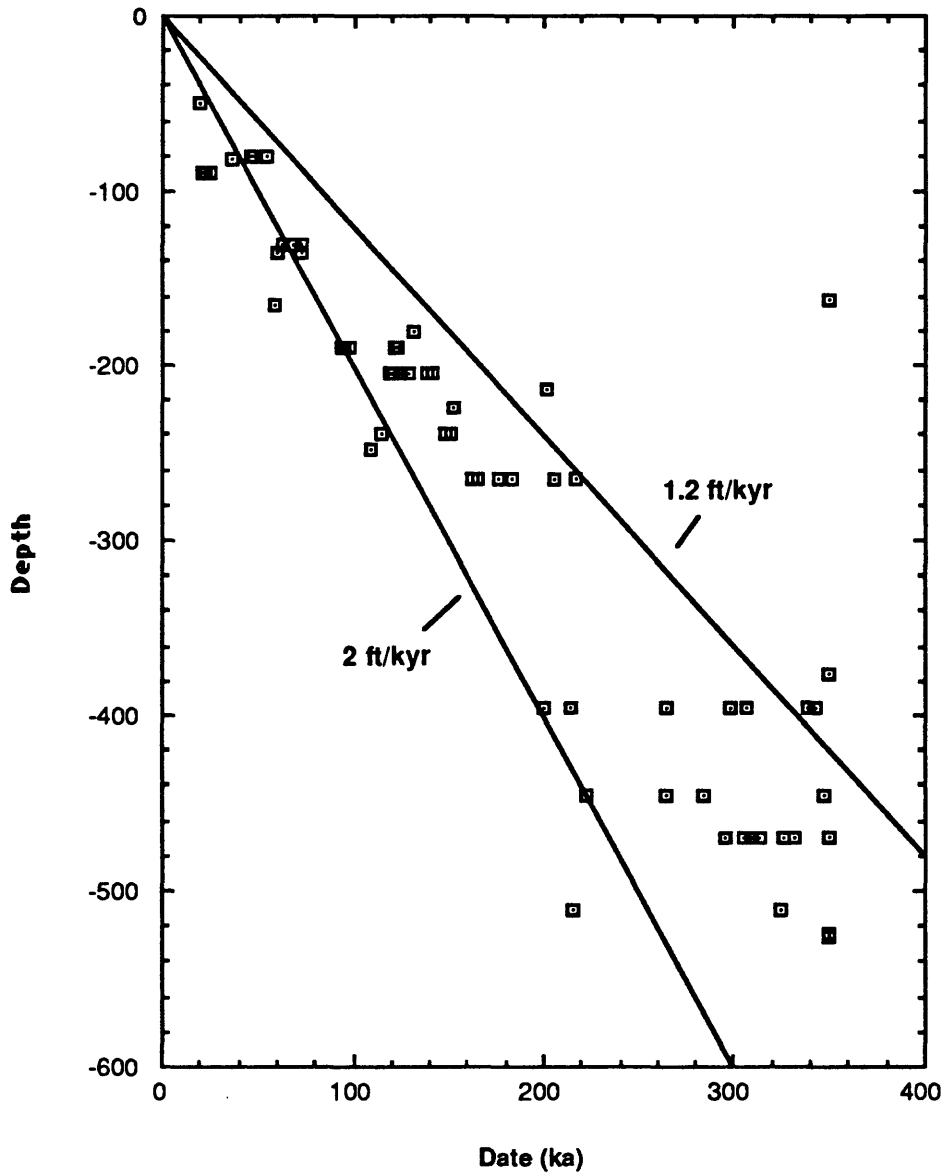

Figure 4

Isochron plot of total dissolutions of halite sample from 80.7' depth in the PAN-3 core. The age error (1s) is based on scatter about the least-squares fit (Schwarcz and Latham, 1989). A: $^{230}Th/^{232}Th$ vs. $^{234}U/^{232}Th$ diagram to determine the $^{230}Th/^{234}U$ activity ratio of the pure authigenic end-member. B: $^{234}U/^{232}Th$ vs. $^{238}U/^{232}Th$ diagram to determine the $^{234}U/^{238}U$ activity ratio of the pure authigenic end-member.

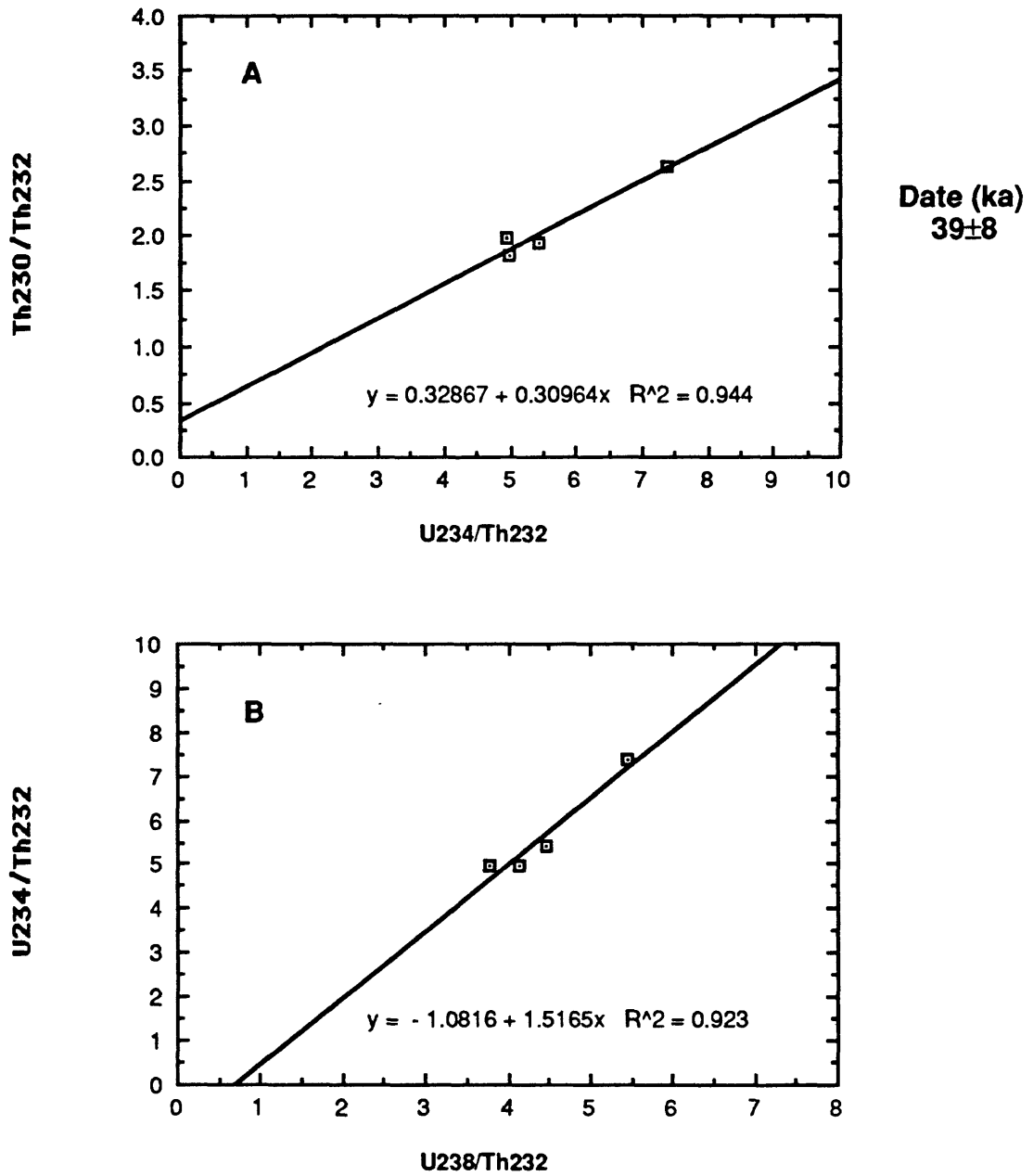

Figure 5

Isochron plot of total dissolutions of halite sample from 90.0' depth in the PAN-3 core. The age error (1s) is based on scatter about the least-squares fit (Schwarcz and Latham, 1989). A: $^{230}Th/^{232}Th$ vs. $^{234}U/^{232}Th$ diagram to determine the $^{230}Th/^{234}U$ activity ratio of the pure authigenic end-member. B: $^{234}U/^{232}Th$ vs. $^{238}U/^{232}Th$ diagram to determine the $^{234}U/^{238}U$ activity ratio of the pure authigenic end-member.

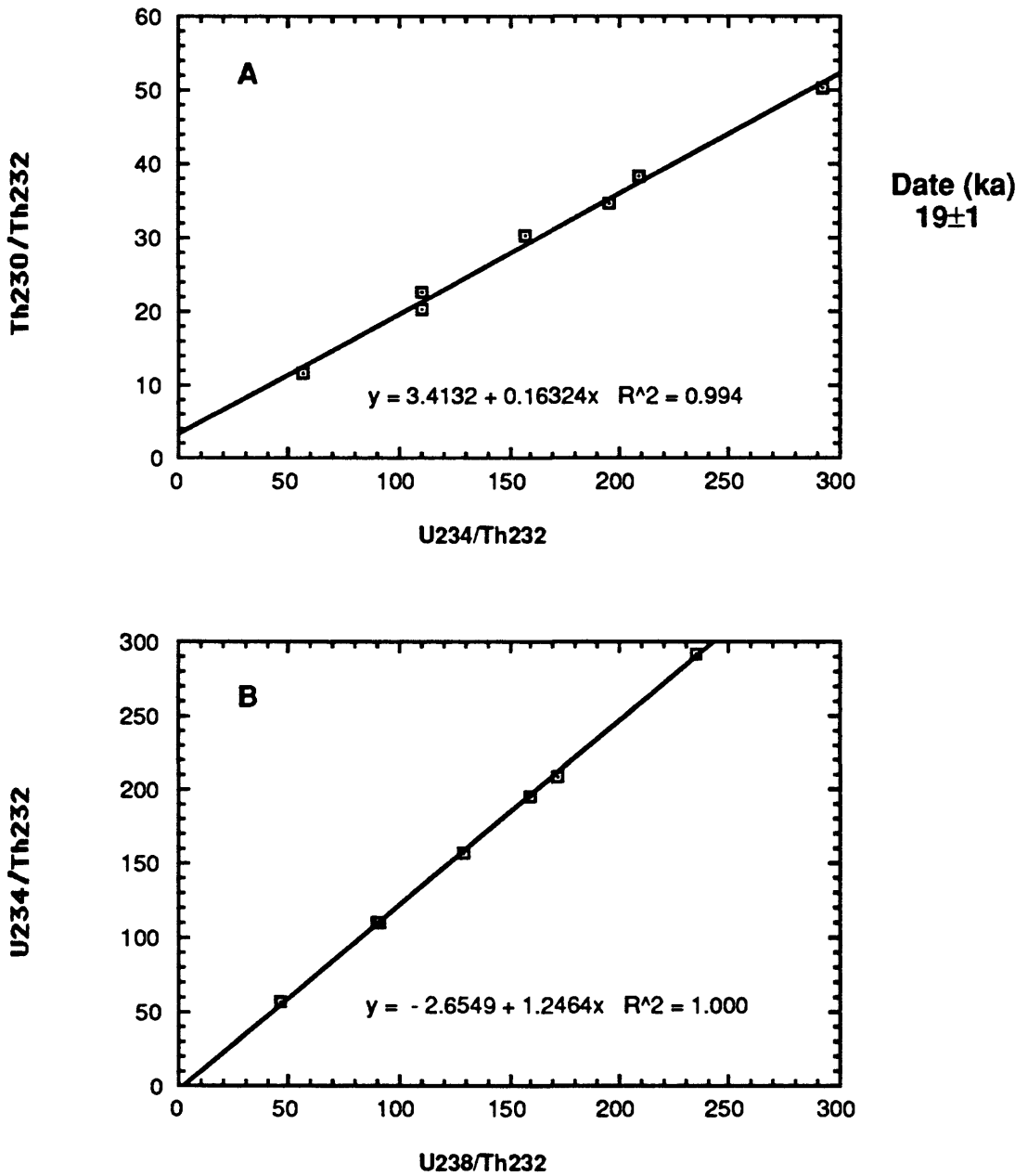

Figure 6

Isochron plot of total dissolutions of halite sample from 131.0' depth in the PAN-3 core. The age error (1s) is based on scatter about the least-squares fit (Schwarcz and Latham, 1989). A: $^{230}Th/^{232}Th$ vs. $^{234}U/^{232}Th$ diagram to determine the $^{230}Th/^{234}U$ activity ratio of the pure authigenic end-member. B: $^{234}U/^{232}Th$ vs. $^{238}U/^{232}Th$ diagram to determine the $^{234}U/^{238}U$ activity ratio of the pure authigenic end-member.

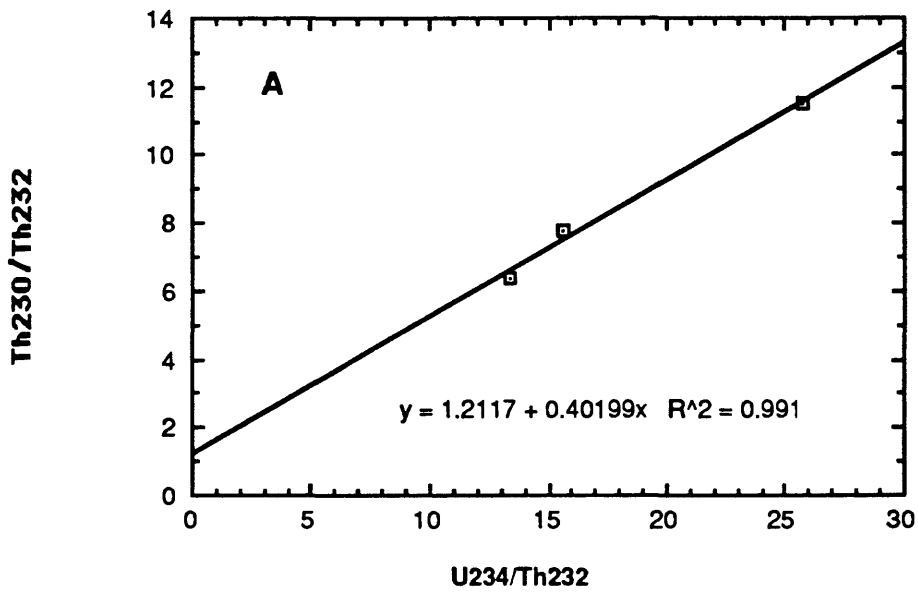

Date (ka)
55±7

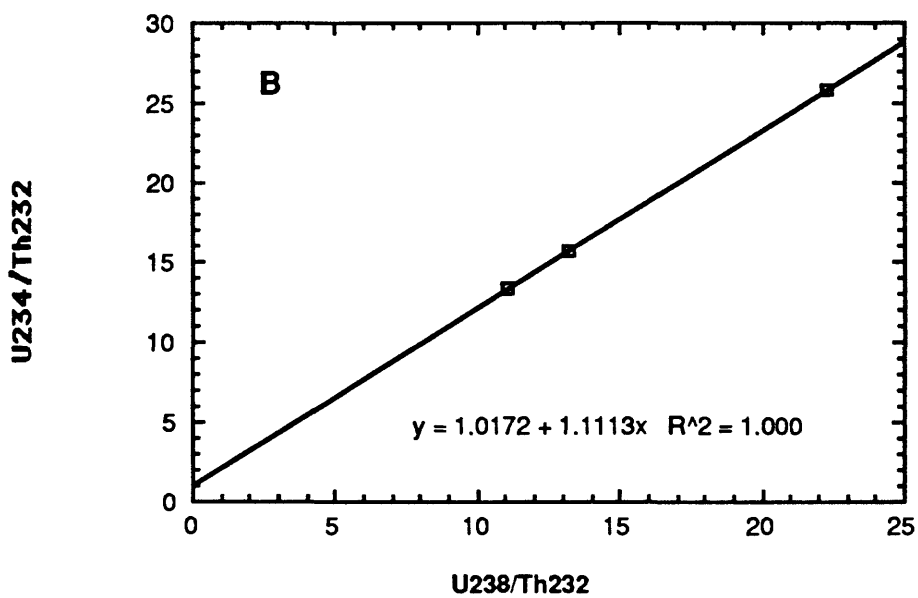

Figure 7

Isochron plot of total dissolutions of halite sample from 190.0' depth in the PAN-3 core. The age error (1s) is based on scatter about the least-squares fit (Schwarcz and Latham, 1989). A: $^{230}Th/^{232}Th$ vs. $^{234}U/^{232}Th$ diagram to determine the $^{230}Th/^{234}U$ activity ratio of the pure authigenic end-member. B: $^{234}U/^{232}Th$ vs. $^{238}U/^{232}Th$ diagram to determine the $^{234}U/^{238}U$ activity ratio of the pure authigenic end-member.

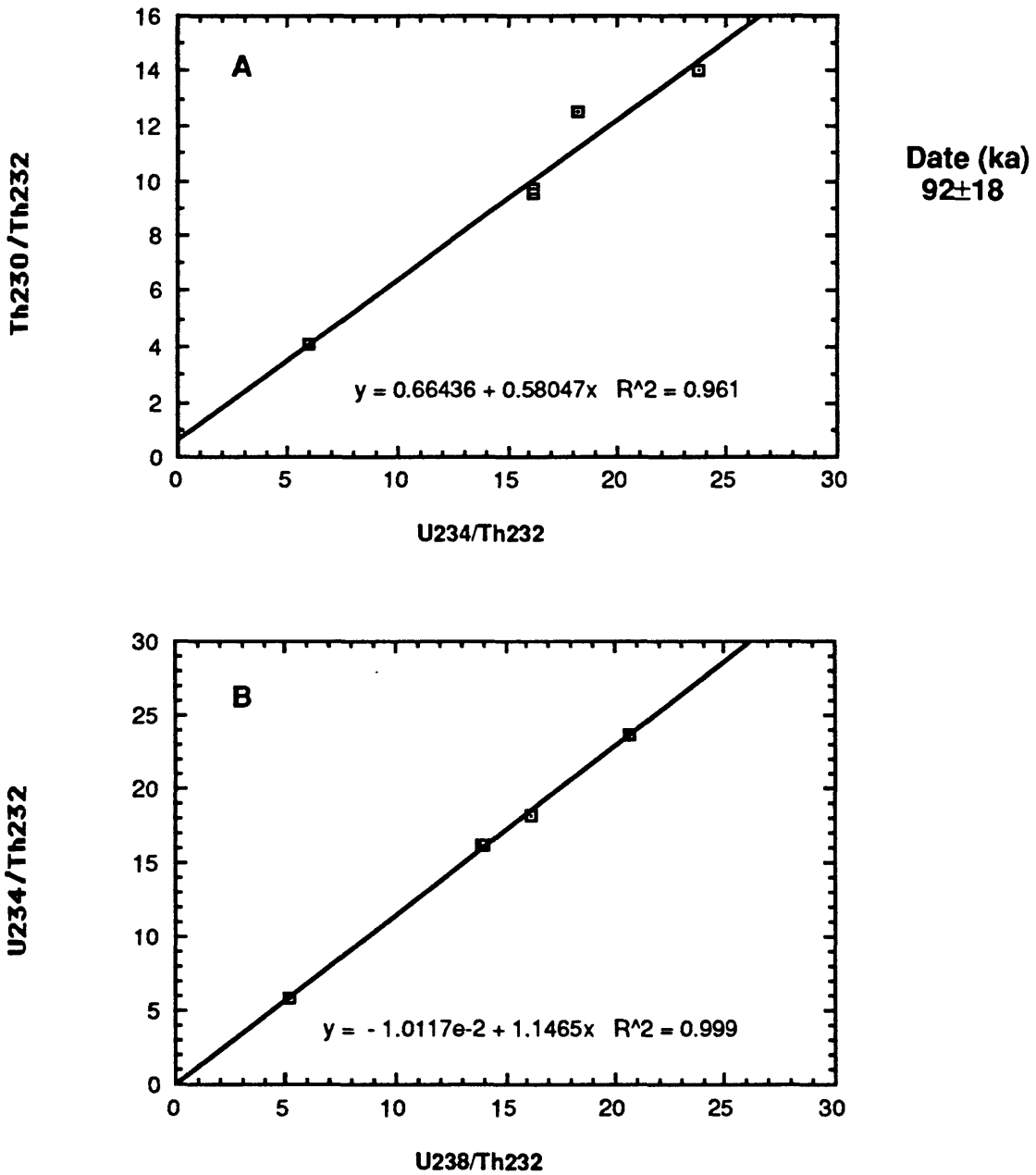

Figure 8

Isochron plot of total dissolutions of halite sample from 205.0' depth in the PAN-3 core. The age error (1s) is based on scatter about the least-squares fit (Schwarcz and Latham, 1989). A: $^{230}Th/^{232}Th$ vs. $^{234}U/^{232}Th$ diagram to determine the $^{230}Th/^{234}U$ activity ratio of the pure authigenic end-member. B: $^{234}U/^{232}Th$ vs. $^{238}U/^{232}Th$ diagram to determine the $^{234}U/^{238}U$ activity ratio of the pure authigenic end-member.

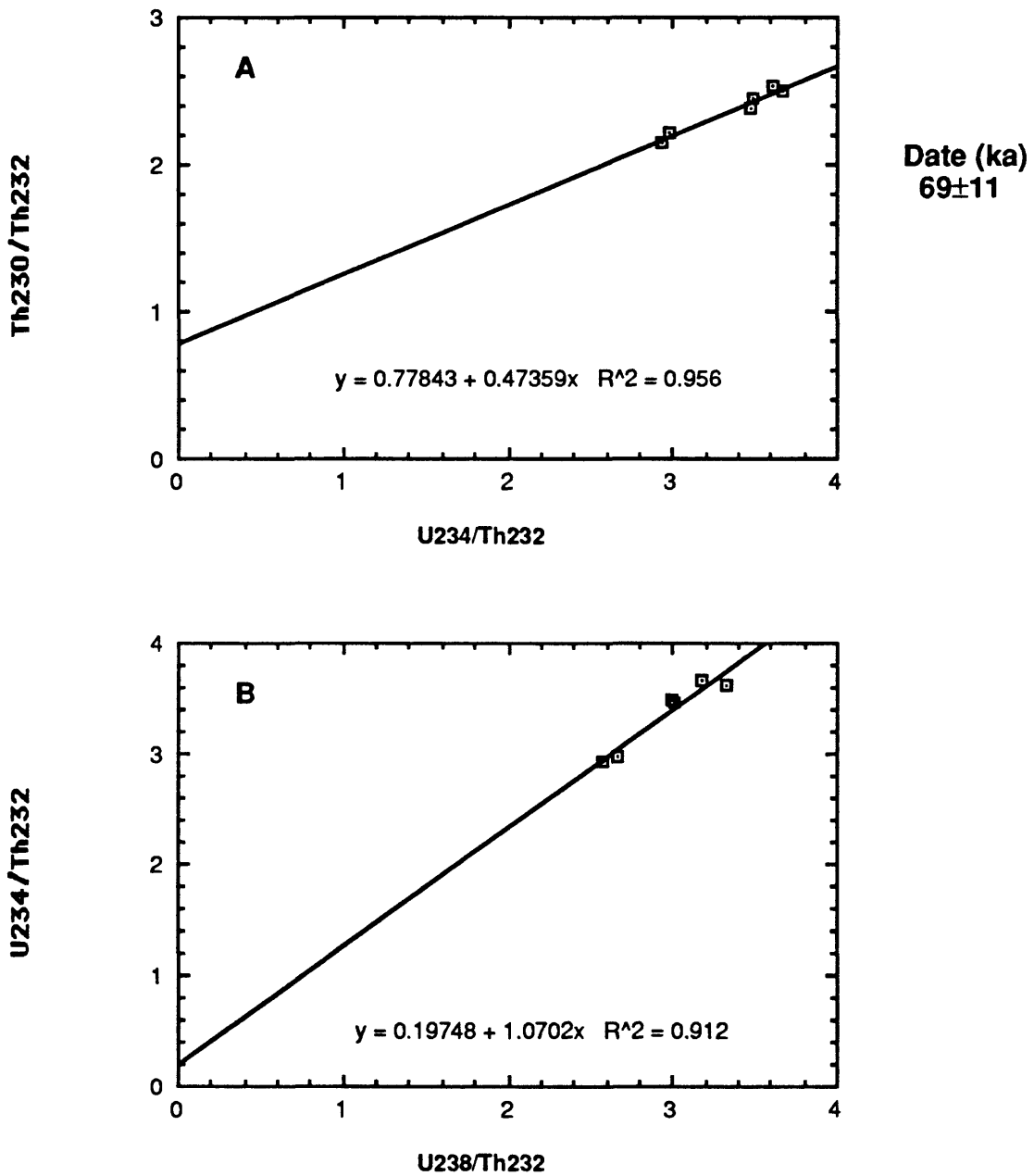

Figure 9

Isochron plot of total dissolutions of halite sample from 239.5' depth in the PAN-3 core. The age error (1s) is based on scatter about the least-squares fit (Schwarcz and Latham, 1989). A: $^{230}Th/^{232}Th$ vs. $^{234}U/^{232}Th$ diagram to determine the $^{230}Th/^{234}U$ activity ratio of the pure authigenic end-member. B: $^{234}U/^{232}Th$ vs. $^{238}U/^{232}Th$ diagram to determine the $^{234}U/^{238}U$ activity ratio of the pure authigenic end-member.

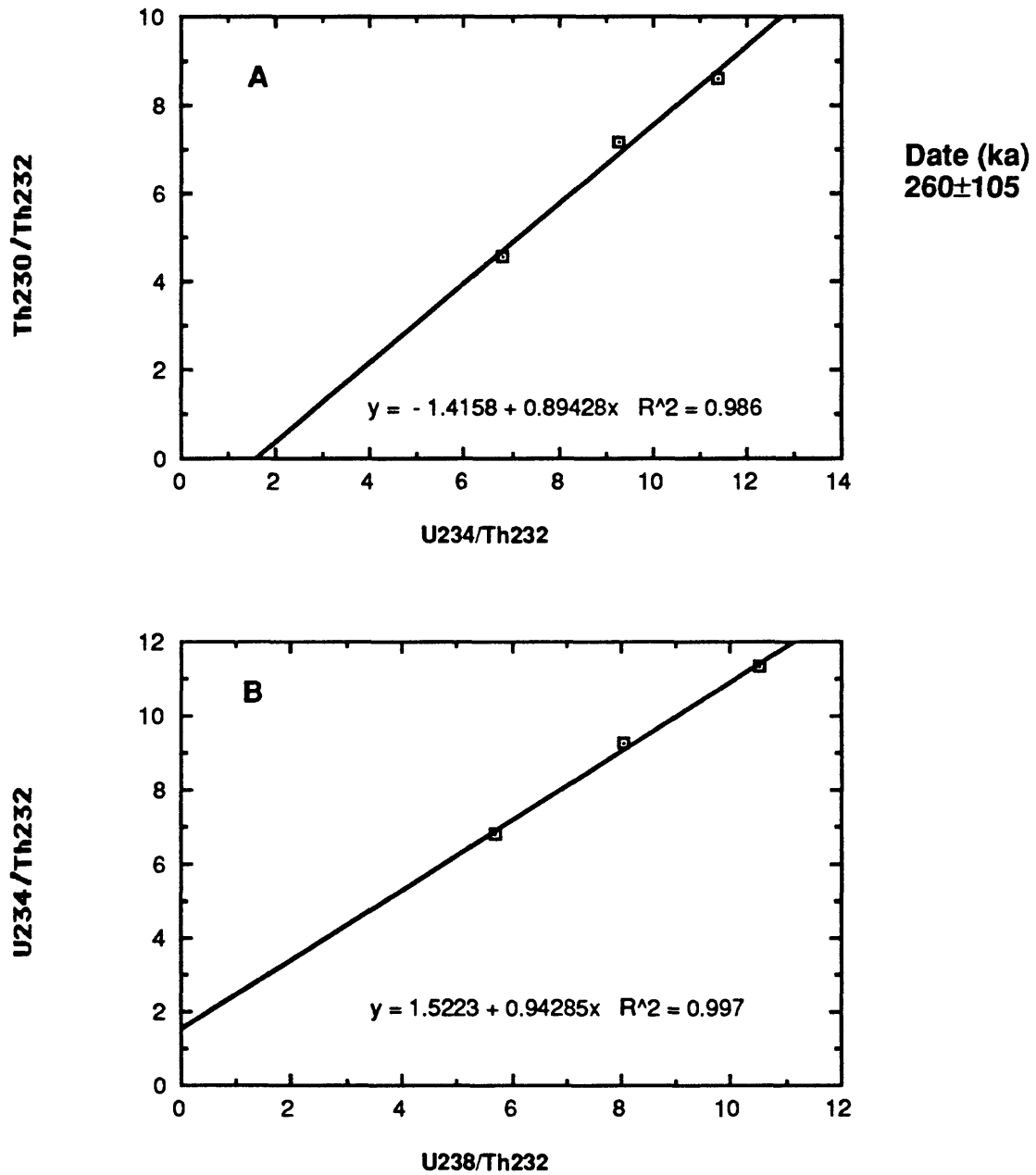

Figure 10

Isochron plot of total dissolutions of halite sample from 265.0' depth in the PAN-3 core. The age error (1s) is based on scatter about the least-squares fit (Schwarcz and Latham, 1989). A: $^{230}Th/^{232}Th$ vs. $^{234}U/^{232}Th$ diagram to determine the $^{230}Th/^{234}U$ activity ratio of the pure authigenic end-member. B: $^{234}U/^{232}Th$ vs. $^{238}U/^{232}Th$ diagram to determine the $^{234}U/^{238}U$ activity ratio of the pure authigenic end-member.

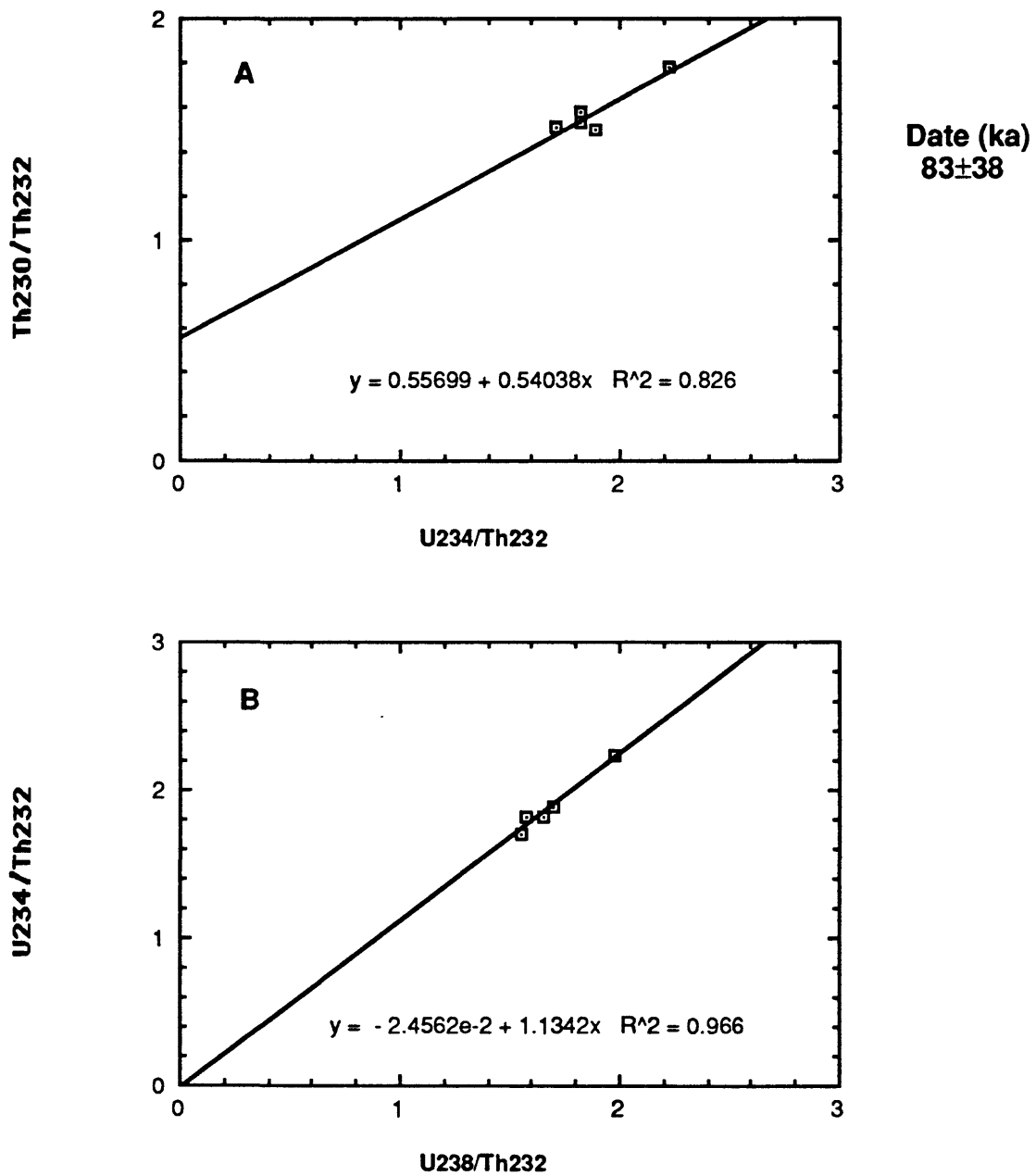

Figure 11

Isochron plot of total dissolutions of gypsum sample from 395.0' depth in the PAN-3 core. The age error (1s) is based on scatter about the least-squares fit (Schwarcz and Latham, 1989). A: $^{230}Th/^{232}Th$ vs. $^{234}U/^{232}Th$ diagram to determine the $^{230}Th/^{234}U$ activity ratio of the pure authigenic end-member. B: $^{234}U/^{232}Th$ vs. $^{238}U/^{232}Th$ diagram to determine the $^{234}U/^{238}U$ activity ratio of the pure authigenic end-member.

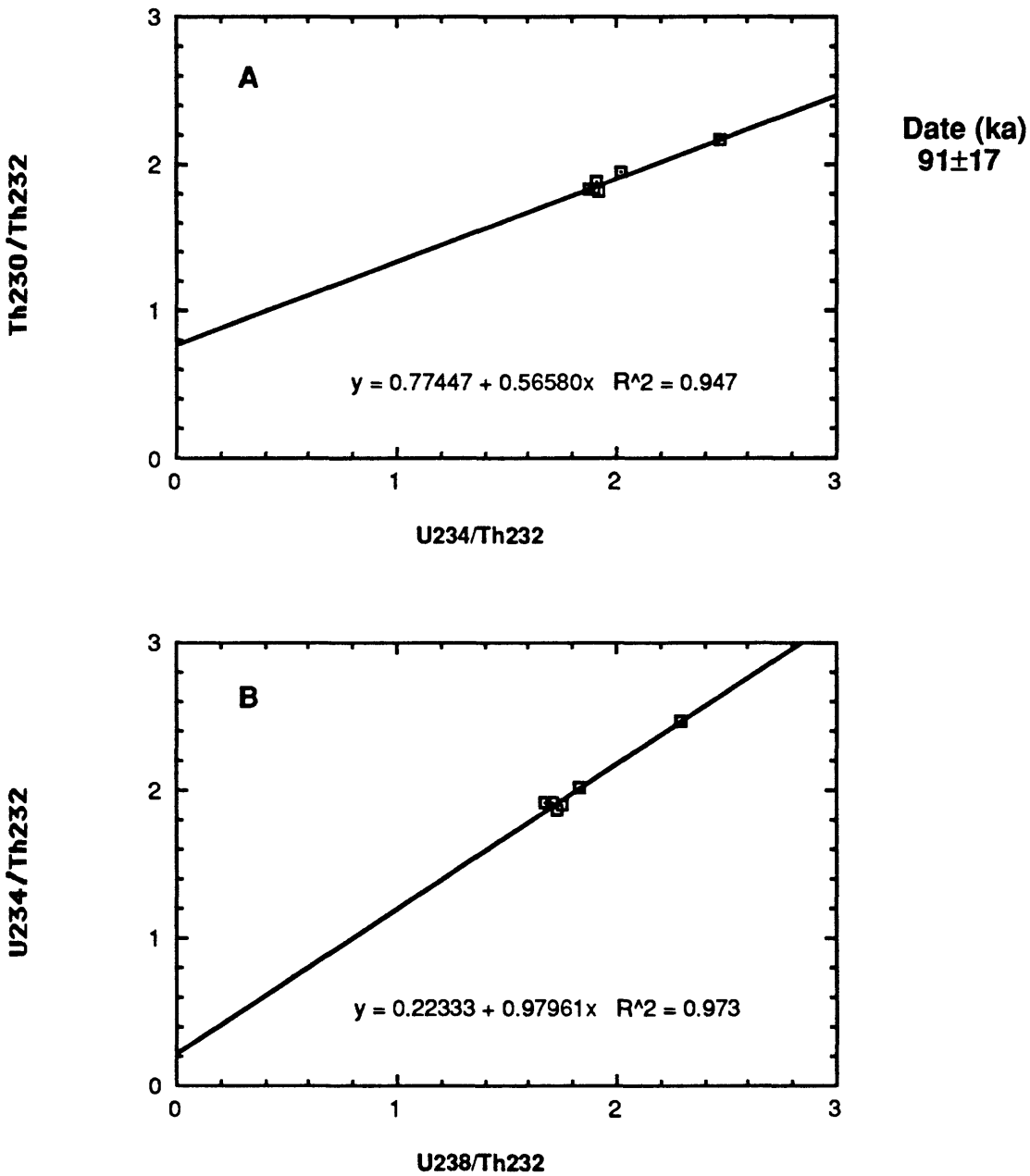

Figure 12

Isochron plot of total dissolutions of halite sample from 445.0' depth in the PAN-3 core. The age error (1s) is based on scatter about the least-squares fit (Schwarcz and Latham, 1989). A: $^{230}Th/^{232}Th$ vs. $^{234}U/^{232}Th$ diagram to determine the $^{230}Th/^{234}U$ activity ratio of the pure authigenic end-member. B: $^{234}U/^{232}Th$ vs. $^{238}U/^{232}Th$ diagram to determine the $^{234}U/^{238}U$ activity ratio of the pure authigenic end-member.

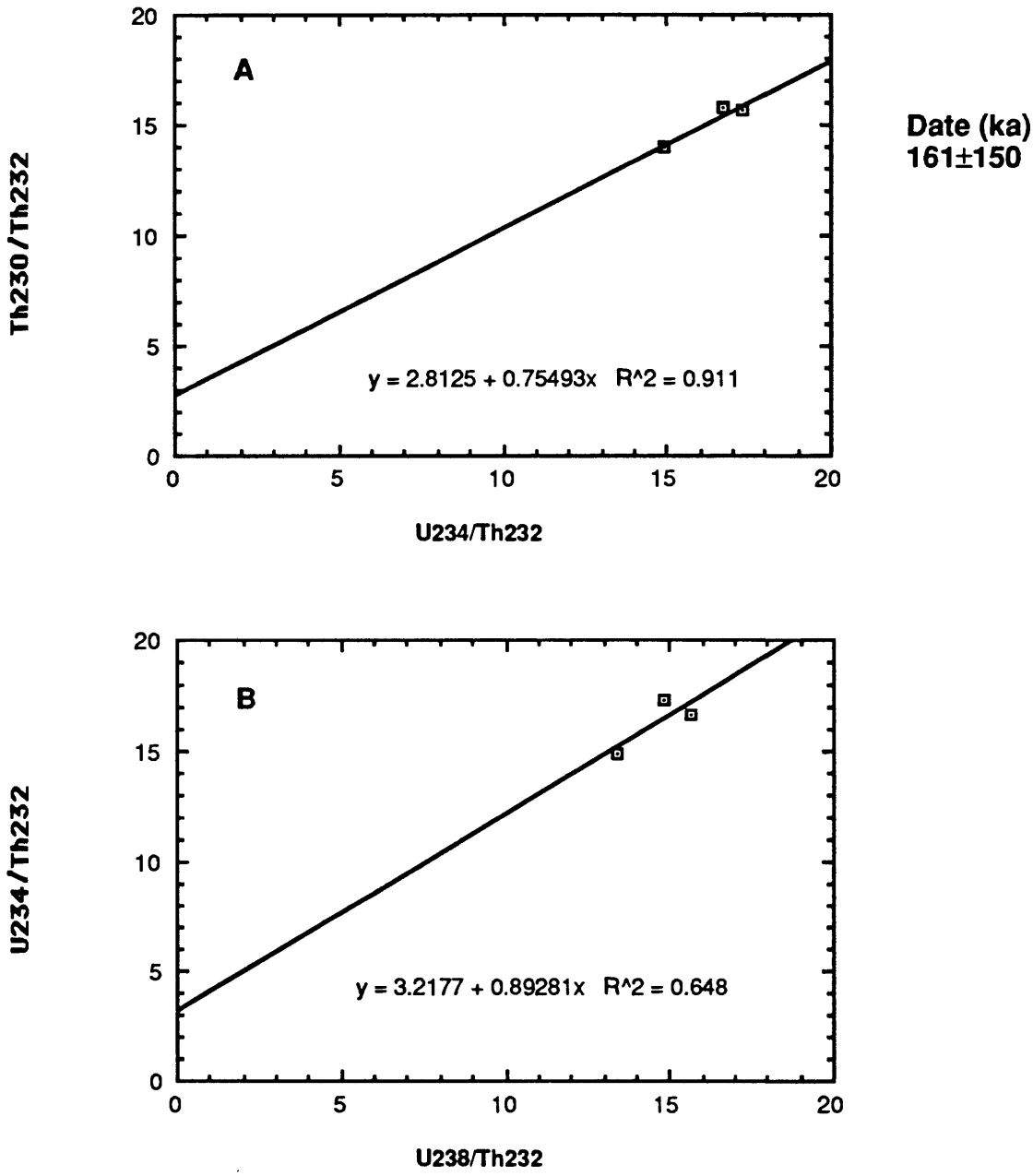

Figure 13

Isochron plot of total dissolutions of halite sample from 470.0' depth in the PAN-3 core. The age error (1s) is based on scatter about the least-squares fit (Schwarcz and Latham, 1989). A: $^{230}Th/^{232}Th$ vs. $^{234}U/^{232}Th$ diagram to determine the $^{230}Th/^{234}U$ activity ratio of the pure authigenic end-member. B: $^{234}U/^{232}Th$ vs. $^{238}U/^{232}Th$ diagram to determine the $^{234}U/^{238}U$ activity ratio of the pure authigenic end-member.

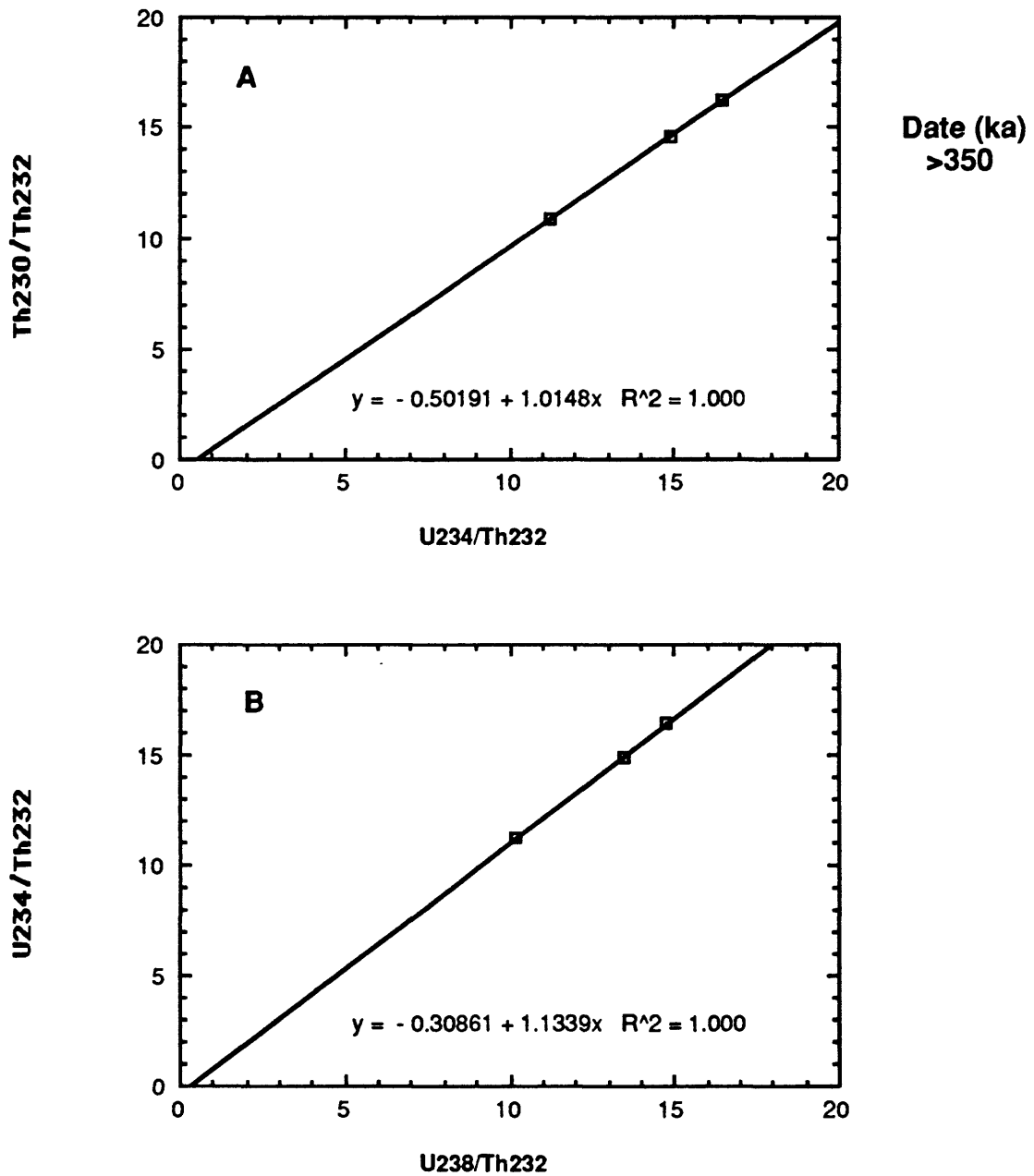

Figure 14

Isochron plot of total dissolutions of halite sample from 470.3' depth in the PAN-3 core. The age error (1s) is based on scatter about the least-squares fit (Schwarcz and Latham, 1989). A: $^{230}Th/^{232}Th$ vs. $^{234}U/^{232}Th$ diagram to determine the $^{230}Th/^{234}U$ activity ratio of the pure authigenic end-member. B: $^{234}U/^{232}Th$ vs. $^{238}U/^{232}Th$ diagram to determine the $^{234}U/^{238}U$ activity ratio of the pure authigenic end-member.

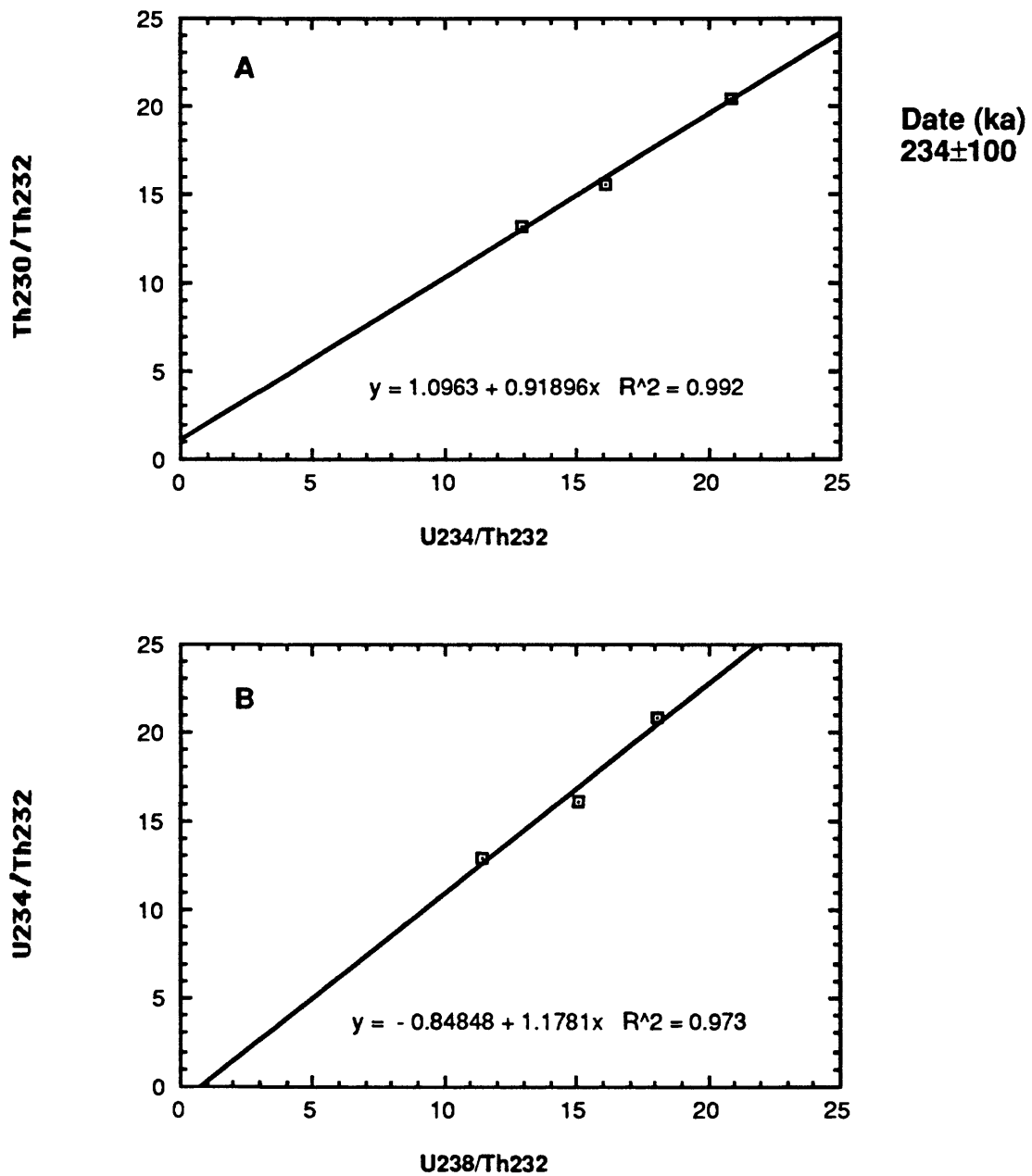

Figure 15

Isochron, best nominal ($^{230}Th/^{232}Th$ ratios >8), and Jannik et al. (1991) ^{36}Cl dates versus depth from analysis of samples from the PAN-3 core. Sedimentation-rate curves of1.2 ft/kyr and 2 ft/kyr are shown for comparison with Figure 3.

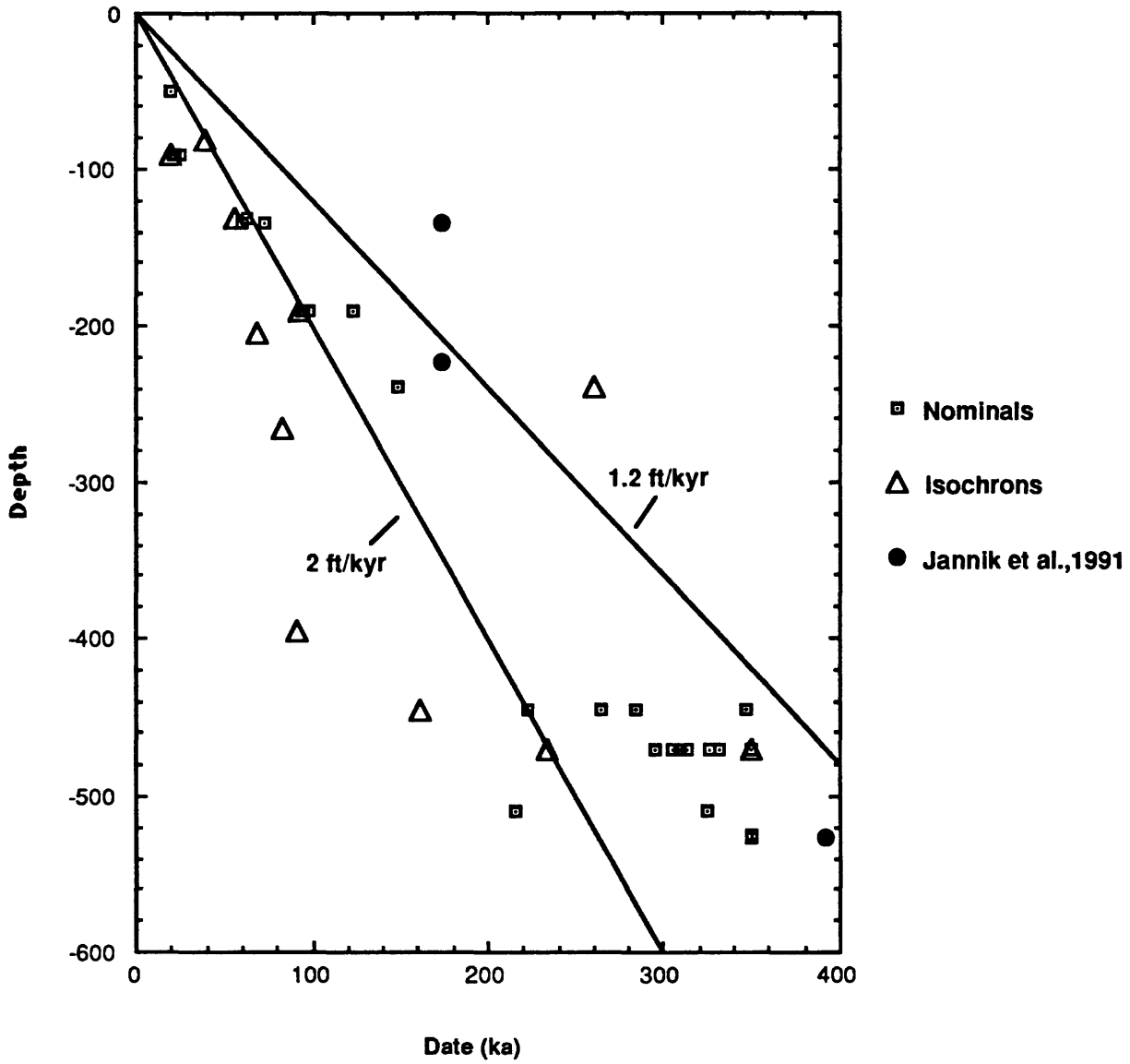

The nominal dates derived from the isotopic analyses are plotted vs. depth in Fig. 3. Samples with dates greater than the range of the technique (> 350 ka) are plotted at 350 ka. The broad trend of increasing sample age with increasing depth has been bracketed by two sedimentation rate curves corresponding to 1.2 ft/kyr and 2 ft/kyr. Approxiimately 70 percent of the analyses fall within this sedimentation-rate envelope. A number of the analyses are of high quality ($^{230}Th/^{232}Th$ ratios > 8), but only the 90-ft sample replicates exhibit nominal dates wihiin error of each other. Replicate analyses from 445 ft to 510 ft display significant variability in nominal dates, outside of error in a number of cases, even though thorium ratios are favorable. Such variability is likely due to localized uranium mobility.

Isochrons were constructed for ten samples (Fig. 4-Fig. 14). The linearity of the $^{230}Th/^{232}Th$ vs. $^{234}U/^{232}Th$ plot shows moderate variability among the samples (R^2 of 0.83-1.00). Generally, those samples with R^2 values greater than 0.95 offer the highest confidence. The isochron dates, the cleanest nominal dates ($^{230}Th/^{232}Th$ ratios > 8), and the Jannik et al. (1991) dates are plotted versus depth in Fig. 15. Sedimentation curves of 1.2 ft/kyr and 2 ft/kyr have been added for comparison with Fig. 3.

There is a general relationship of age with depth in plots Fig. 3 and Fig. 15, but unfortunately, the scatter exhibited allows only the broadest interpretation of sedimentation rates. It is likely that localized uranium migration among these extremely soluble halites is the cause of poor precision among the analyses, poor isochron linearity, and apparent age reversals which are ultimately manifested as scatter on the depth versus age plots. The ^{36}Cl dates of Jannik et al. (1991) generally fall within the sedimentation-rate trend defined by our analyses. Our analyses are generally bracketed between sedimentation-rate curves of 1.2 ft/kyr and 2 ft/kyr. A sedimentation rate of 1.2 ft/kyr would result in an age of 830 ka at the 1000 foot bottom of the core and a sedimentation rate of 2 ft/kyr would result in an age of 500 ka at the bottom of the core. The locally ubiquitous Bishop Tuff (age=758±2 kyr) is not present in this core suggesting either its local nondeposition, erosion, or existence deeper in the basin. The last possibility in conjunction with our U-series ages requires a deposition rate faster than 1.2 ft/kyr.

ACKNOWLEDGEMENTS

The authors appreciate the thoughtful reviews of Bob Rosenbauer and Debbie Trimble.

BIBLIOGRAPHY

Bischoff, J.L. and Fitzpatrick, J. A. (1991) U-series dating of impure carbonates: An isochron technique using total-sample dissolution. *Geochimica et Cosmochimica Acta* **55** 543-554.

Bischoff, J.L., Rosenbauer, R.J., de Lumley, H., and Tavoso, A. (1988) A test of Uranium-series dating of fossil tooth enamal: results from Tournal Cave, France. *Applied Geochemistry* **3** 145-151.

Bischoff, J.L., Rosenbauer, R.J., and Smith, G.I. (1985) Uranium-Series dating of sediments from Searles Lake, California: differences between continental and marine climate records.*Science* **227** 1222-1221.

Fitzpatrick, J.A. and Bischoff, J.L. (1993) Uranium-Series dates on sediments of the high shoreline of Panamint Valley, California. U.S. Geological Survey open-file report 93-232.

Jannik, N.O., Phillips, F.M., Smith, G.I., and Elmore, D. (1991) A ^{36}Cl chronology of lacustrine sedimentation in the Pleistocene Owens River system. *Geological Society of America Bulletin* **103** 1146-1159.

Schwarcz H.P. and Latham A.G. (1989) Dirty calcites 1. Uranium-series dating of contaminated calcite using leachates alone. *Chem. Geol.* **80** 35-43.

Smith, G.I. (1984) Paleohydrologic regimes in the Southwestern Great Basin, 0-3.2 my ago, compared with other long records of "Global" climate. *Quat. Res.* **22** 1-17.

Smith, G.I. and Pratt, W.P. (1957) Core logs from Owens, China, Searles, and Panamint Basins California. U.S. Geological Suvey Bulletin 1045-A.

Smith R.S. (1976) *Late-Quaternary pluvial and tectonic history of Panamint Valley, Inyo and San Bernardino Counties, California.* Ph.D. dissertation, California Institute of Technology 295p.